Backbone of conductivity in two-dimensional metal-insulator composites

Backbone of conductivity in two-dimensional metal-insulator composites

Joakim Reuteler, Markus Hütter, and Ludwig J. Gauckler

Citation: J. Appl. Phys. **110**, 024909 (2011); doi: 10.1063/1.3610402
View online: http://dx.doi.org/10.1063/1.3610402
View Table of Contents: http://jap.aip.org/resource/1/JAPIAU/v110/i2
Published by the American Institute of Physics.

Backbone of conductivity in two-dimensional metal-insulator composites

Joakim Reuteler,[1,a)] Markus Hütter,[2,b)] and Ludwig J. Gauckler[1]
[1]*ETH Zurich, Department of Materials, Nonmetallic Inorganic Materials, 8093 Zürich, Switzerland*
[2]*Eindhoven University of Technology, Mechanical Engineering, Materials Technology, 5600 MB Eindhoven, The Netherlands*

(Received 9 March 2011; accepted 10 June 2011; published online 29 July 2011)

In percolation theory, the backbone is defined by chopping off dangling ends from the percolating cluster. For structures with high degree of spatial correlation, as they are typical for porous thin films, trimming of the full structure to reveal the part determining the electrical conductivity is more subtle than the classic definition of the backbone. To expand the applicability of the concept, we present a purely geometric definition for the backbone of a two-dimensional percolating cluster. It is based on a sequence of image analysis operations defining the backbone in terms of an image filter. The change of both area fraction and effective conductivity induced by applying the backbone filter to various binary images and a two-parameter family of sets is assessed by numerical means. It is found that the backbone filter simplifies the geometry of complex microstructures significantly and at the same time preserves their electrical DC behavior. We conclude that the backbone will be useful as a first ingredient for a geometric estimator of the effective conductivity of metal-insulator composites. © *2011 American Institute of Physics*. [doi:10.1063/1.3610402]

I. INTRODUCTION

At the heart of material science is the development of materials with improved properties. Nowadays many industrially relevant materials belong to the class of composite materials. Based on trial and error, compositions and processing have been optimized. There is no doubt that the microstructure has a crucial influence on the properties of composites. However, there is a lack in theoretical knowledge for relating the microstructure to the properties of such materials.[1]

Metallic thin films are employed in various miniaturized devices ranging from microelectronics and micromechanics to miniaturized fuel cells. In particular the electrodes of nowadays best performing low temperature miniaturized solid oxide fuel cells consist of porous platinum thin films.[2,3] These films have a lateral extension larger than 100 μm, a thickness in the range of 100 nm and are flat in the simplest case. Typically they are deposited by magnetron sputtering in a low pressure argon atmosphere. The Pt grains grow in columnar fashion yielding a quasi two-dimensional microstructure. The influence of the microstructure of such electrodes on cell performance is very complex. Thermal stability, amount of electrochemically active sites as well as electrical conductivity have to be optimized. In this study we focus on the electrical conductivity of two-dimensional metal-insulator composites.

We start with a brief review of the notion of composites and explain the relation to binary images. Then we derive the boundary value problem describing electrical conductivity. We briefly discuss present theories describing the effective conductivity of metal-insulator composites. Then we review in detail the definition of the backbone and state the main finding of this study.

A. Metal-insulator composites

Composite materials consist of a mixture of at least two immiscible phases. Typically the different phases are finely dispersed but the regions occupied by one phase are still large compared to the atomic length scale. The heterogeneous nature becomes apparent in the microscopic range. On the macroscopic scale such composites behave as if they were one-phase materials. This means that there is a length scale such that all samples of the composite larger than a square of this length have statistically the same properties. This idea is closely related to the definition of a so-called representative volume element of a composite. A rigorous study of the approximations adopted by this approach was given by Sab.[4] Therein a practical procedure for determining the effective properties of a composite with microstructure modeled by a random field is given. The properties observed at the macroscopic scale are called effective properties. They are determined by three factors: the properties of the phases, the properties of the interfaces, and the spatial arrangement of the phases. The latter is called microstructure and is exactly what makes composites so attractive: properties can be combined and tuned by altering the microstructure. In a composite it is even possible to obtain properties which never can be observed in one-phase materials.[5]

In this study, we consider macroscopically homogeneous two-dimensional metal-insulator composites. The property we investigate is the effective electrical conductivity. We assume that the interface between the metal and the insulator does not develop a conductivity higher than that of the metal, and can hence be neglected. Fixing the conductivity

[a)]Electronic mail: joakim.reuteler@mat.ethz.ch.
[b)]Formerly with ETH Zurich, Department of Materials, Polymer Physics, 8093 Zürich, Switzerland.

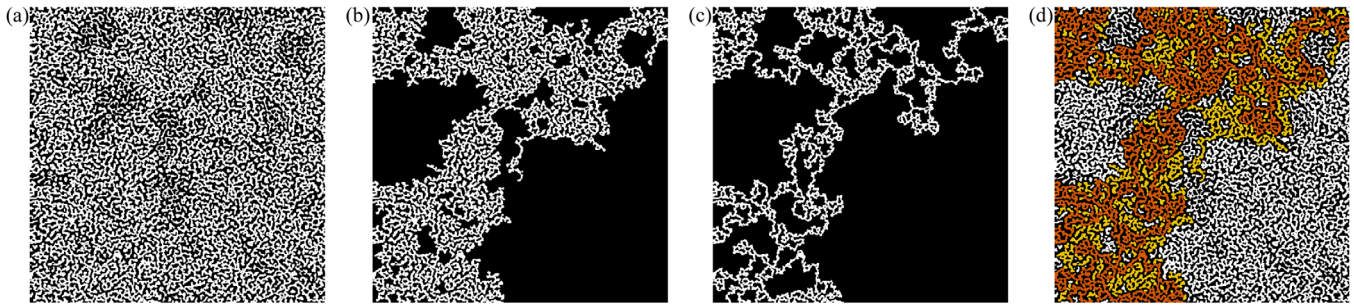

FIG. 1. (Color online) (a) Sample of metal-insulator composite represented by a binary image. White pixels represent the metal and black pixels the insulating phase. (b) Percolating cluster of the metal phase obtained by removing isolated islands. (c) Backbone of the percolating cluster obtained by chopping off dead-ends according to the definition presented in this study. (d) Visualization of this division of the metal phase: white for isolated islands, yellow for dead-ends and orange for the backbone.

of the metal phase we are interested in the relation between the effective conductivity and the microstructure.

A sample of a metal-insulator composite is a rectangle W with a subset $M \subset W$ that represents the space occupied by the metal phase. The complement M^c is the space occupied by the insulator. A binary image is a discrete representation of such a sample. The white pixels approximate the metal phase and the black pixels approximate the space occupied by the insulator. We thus can interpret any binary image as a sample of a metal-insulator composite. Figure 1(a) shows an example of such a sample. Actually, this image is a thresholded scanning electron micrograph of an agglomerated Pt thin film deposited on a ceramic substrate. The width of the metal rods is in the range of 200 nm.

B. Effective conductivity

The effective electrical conductivity σ_e of a square sample is determined experimentally by applying a voltage drop V on opposing edges and measuring the current I that flows [Fig. 2(a)]. In two dimensions the effective conductivity is defined by

$$\sigma_e = \frac{I}{V}. \tag{1}$$

The physics of the measurement of the effective conductivity is described by the Maxwell equations[6]

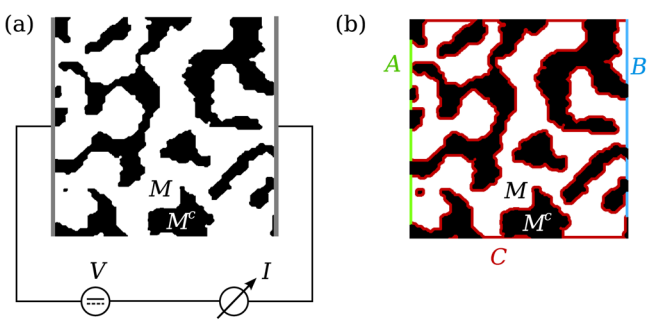

FIG. 2. (Color online) (a) Experimental setup for measurement of the horizontal effective conductivity of a metal-insulator composite. (b) Geometry of the boundary value problem describing the physics of the measurement of the effective conductivity.

$$\begin{aligned} \nabla \cdot \mathbf{E} &= 4\pi\rho \\ \nabla \times \mathbf{E} &= -\frac{\partial}{\partial t}\mathbf{B} \\ \nabla \cdot \mathbf{B} &= 0 \\ \nabla \times \mathbf{B} &= \frac{1}{c}\frac{\partial}{\partial t}\mathbf{E} + 4\pi\mathbf{j}, \end{aligned} \tag{2}$$

where $\mathbf{E}$ is the electric field, ρ is the charge density, $\mathbf{B}$ is the magnetic induction and $\mathbf{j}$ is the current density. In the present case all time dependent terms can be dropped. Thus the electric field $\mathbf{E}$ has a potential u, i.e., $\mathbf{E} = \nabla u$. The subset $M \subset W$ is the space occupied by metal, its left boundary is denoted A and its right boundary is B. The remaining boundary of the metal is denoted $C = \partial M \backslash (A \cup B)$, see Fig. 2(b). The divergence of the last Maxwell equation shows that the current density is solenoidal, i.e.,$\nabla \cdot \mathbf{j} = 0$. This implies that no current flows across the boundary C, i.e., $\mathbf{n} \cdot \mathbf{j} = 0$ on C, where $\mathbf{n}$ denotes the normal vector on C. To see this, consider a box of width $\varepsilon > 0$ around a piece of the boundary and integrate the divergence of the current density. Apply Gauss' theorem and then let $\varepsilon \to 0$. Within a metal the current density is proportional to the electric field, i.e., $\mathbf{j} = \sigma \nabla u$ (Ohm's law), where $\infty > \sigma > 0$ is the isotropic and constant conductivity of the metal. Thus we get $\mathbf{n} \cdot \nabla u = 0$ on C. Within the metal M we have $0 = \nabla \cdot \mathbf{j} = \nabla \cdot \sigma \nabla u = \sigma \Delta u$. Considering all this, we get the following boundary value problem

$$\begin{aligned} &\Delta u = 0, \text{ on } M \\ &\mathbf{n} \cdot \nabla u = 0, \text{on } C \\ &u = 0, \text{ on } A \\ &u = V, \text{ on } B \end{aligned} \tag{3}$$

for the electric potential u. The total current through the sample is $I = \sigma \int_B \mathbf{n} \cdot \nabla u \, do$. Using Eq. (1) the effective conductivity is given by

$$\sigma_e = \sigma \frac{\int_B \mathbf{n} \cdot \nabla u \, do}{V}. \tag{4}$$

We now derive an alternative expression for the effective conductivity from Eq. (4). Without changing the value of the integral we can replace the integrand by $(1/V)u\nabla u \cdot \mathbf{n}$

and extend the integration to the whole boundary of M. Using $\nabla \cdot u\nabla u = |\nabla u|^2 + u\triangle u$ we can apply Gauss' theorem. Since u satisfies the Poisson equation we have shown that the effective conductivity can be computed by the following energy functional

$$\sigma_e = \sigma \frac{\int_M |\nabla u|^2 \mathrm{d}\mu}{V^2}. \tag{5}$$

The dependence of the effective conductivity on the geometry of the metal phase M is implicit for both of these expressions.

C. Theories for the effective conductivity

It is an old problem to describe the effective conductivity of metal-insulator composites in terms of their microstructure.[7] In principle the area fraction and the spatial arrangement of the metal phase determine the effective conductivity. The question is how to reduce this information to one number giving the effective conductivity. Solving the boundary value problem given by Eq. (3) on a computer is limited by the complexity of the set representing the metal phase. There is no way to determine the effective conductivity in an efficient way directly from the microstructure. Various approaches to the problem have been made. We refer to the following monographs[5,8] and the short and transparent review.[9] We now comment on the relevant results.

So called effective medium theories result in expressions which link the area fraction of metal directly to the conductivity. The exact form is determined analytically from assumptions on the microstructure. The expressions from Bruggeman's symmetric and asymmetric media theory can be interpolated yielding a general effective media equation.[9] Interestingly for metal-insulator composites this equation reduces to the expression which is postulated in percolation theory.

In percolation theory[10] the effective conductivity is assumed to follow a power law above the percolation threshold ϕ_c, i.e.,

$$\sigma_{PT}(\phi) = \sigma\left(\frac{\phi - \phi_c}{1 - \phi_c}\right)^t, \tag{6}$$

where ϕ is the area fraction of metal. The critical exponent t should be universal for fixed space dimension. Unfortunately it cannot be computed directly and so has to be determined from fitting Eq. (6) to experimental and simulation data. The percolation threshold ϕ_c depends on the underlying lattice. For two dimensions the values have been determined analytically for the possible lattices. The theory is only valid for the case of structures where each site has a fixed probability to be occupied, independent of all other sites. Therefore in practice both ϕ_c and t are treated as fitting parameters in order to accommodate small deviations from purely uncorrelated random structures.

Using homogenization theory rigorous bounds for the effective conductivity have been derived. Based on information coded in the n-point correlation functions there is a whole hierarchy of nontrivial upper bounds for the effective conductivity. We summarize the review and the formulae given in a monograph by Torquato[8] for the case of a metal-insulator composite in two dimensions. The two-point correlation function yields a bound which, interestingly, only depends on the area fraction ϕ covered by the metal. It reads

$$\sigma^{(2)}(\phi) = \sigma \frac{\phi}{2 - \phi}, \tag{7}$$

and is called upper Hashin-Shtrikman bound.[11,12] The three-point upper bound is much more tedious to compute. Expressions given by Prager[13] and Beran[14] were later simplified: it was shown that the three-point bound can be written using a threefold integral of the three-point correlation function of the metal.[15,16] This functional is often denoted by $\zeta \in [0, 1]$. An algorithm for the computation of ζ from discrete images was reported by Berryman.[17] There seems to be no simple interpretation of ζ.[16] In this notation the three-point bound reads

$$\sigma^{(3)}(\phi, \zeta) = \sigma \frac{\phi\zeta}{1 - \phi + \zeta}. \tag{8}$$

The four point bounds were also computed.[16] In two dimensions the four-point parameters vanish. The upper four-point bound depends only on ϕ and ζ, it reads

$$\sigma^{(4)}(\phi, \zeta) = \sigma \frac{\phi\zeta}{2 - 2\phi + \phi\zeta}. \tag{9}$$

All the corresponding lower bounds are trivial for metal-insulator composites in two-dimensional space.

D. Backbone of conductivity

Only the metal belonging to the percolating cluster can carry a nonzero current density. Thus isolated islands can be neglected. By experiment Last and Thouless showed that the effective conductivity is not proportional to the area fraction of metal in the percolating cluster.[18] Their explanation was that only a small fraction of the sites belonging to the percolating cluster actually carry current. If the percolating cluster represents a resistor network, dangling bonds lead to resistors that carry no current and are dead-ends in this sense. The backbone of the percolating cluster was then defined as the part of the percolating cluster which carries current.[19,20] The way to compute the backbone is left unclear in the latter publications. Later Kirkpatrick defined the backbone to be the maximal biconnected component of the percolating cluster.[21] An algorithm to compute this was already at hand before.[22,23] More efficient algorithms were found later.[24,25] However, this definition of the backbone does not allow for dead-ends with a minimal width larger than one. For example a branch of width two is biconnected to its mother branch because a one pixel wide path can go into it and return without crossing itself. The biconnected component of the percolating cluster in Fig. 1(b) actually is equal to the percolating cluster.

Recently another definition for dead-ends of a set was given by Jørgensen.[26] His definition is based on computing traveling distances when going from one edge to the

opposing one. This is done by solving the Eikonal equation with constant velocity within the foreground. Then the shortest path is reconstructed by back tracing from the destination edge toward the departure edge. The algorithm works in any space dimension. In fact the most direct path is computed, i.e., detours are chopped off. Therefore this definition of "dead-ends" does not generalize the earlier definitions discussed above.

The original definition of the backbone as the current carrying part of the percolating cluster is based on the idea that there are parts of the percolating cluster in which the current density vanishes. This only holds for discrete networks of ideal resistors. Let's assume that a percolating metal cluster in continuous space contained a part that carries no current at all. Mathematically speaking this means that there is an open subset $O \subset M_{\mathrm{PC}}$ within the percolating metal cluster where the current density $\sigma \nabla u$ vanishes. This implies that the potential u is constant in this subset. Since u is the solution of an elliptic partial differential equation it possesses the "unique continuation property" and thus the potential has to be constant on the whole percolating cluster M_{PC}. Consequently the current density vanishes on M_{PC} which is in contradiction to the fact that a percolating cluster will carry current if its ends are subject to a potential drop. Thus the current density in the percolating cluster is zero nowhere. So by the original definition the backbone is equal to the percolating cluster. In other words dead-ends do not exist, there are only broadened rods carrying lower current density. Looking at Eq. (5) we see that the effective conductivity can only decrease if parts of the percolating cluster are truncated. We found a subset of the percolating cluster whose effective conductivity is only slightly smaller.

In the remainder of this paper we present an algorithm based on image analysis operations, which is able to reduce the percolating cluster significantly in mass while leaving the effective conductivity essentially constant. In this sense we give a geometrical definition of the backbone of conductivity. An example of the result of applying our algorithm is shown in Fig. 1(c). The invariance of the effective conductivity is observed for various samples represented by binary images and a two-parameter family of sets, see Figs. 3 and 4(c). In contrast to the original definition of the backbone as used in percolation theory our definition contains the case of dead-ends of arbitrary width. Therefore the backbone of the percolating cluster shown in Fig. 1(b) is a proper subset according to our definition. The backbone as defined by Jørgensen is more restrictive than the one presented here. His definition frees the percolating cluster from all detours, whereas our backbone may contain detours as long as the starting and end point are separate. See the loops in Fig. 1(c) on the upper right side.

For the purpose of this study it is irrelevant if the binary images are smaller than the representative volume element of the random sets they were taken from.

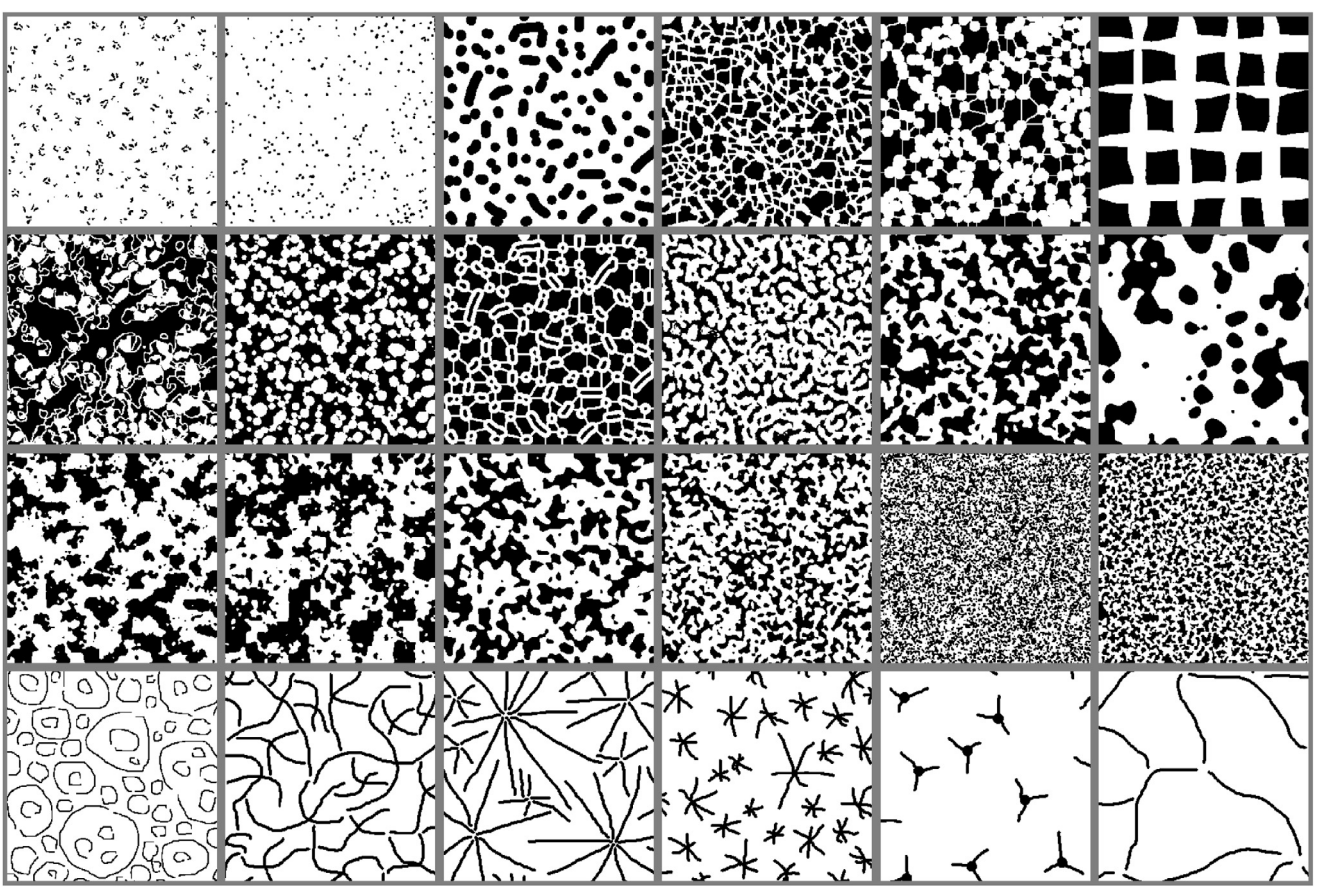

FIG. 3. Montage of the binary images representing metal-insulator composites investigated in this study. In all images the metal phase is represented by white.

II. METHODS

Samples of metal-insulator composites are the basis of this study. On the one hand we use binary images with the size of 500×500 pixels (Fig. 3). These images were obtained from microscopy, simulation of random fields, and freehand drawing. The aim was to generate a broad range of microstructures. On the other hand we use square symmetric subsets of the unit square [Fig. 4(a)]. They are determined by two parameters, the width of the rods ensuring percolation and the side length of the central square. The width of the rods a was varied at equal steps of 0.2 from 0.1 to 0.9 in units of the side length of the image window. For each such value the range of the side length of the central square b was varied between a and the side length of the image window. For each of the five values of a, parameter b was chosen to take on 20 equally spaced values. Some examples of sets obtained by varying the two parameters are given in Fig. 4(c). It will become clear in Sec. III that the pairs (ϕ,σ_e) obtained from such sets cover a large fraction of all combinations attainable by macroscopically isotropic metal-insulator composites.

A. Computing the effective conductivity

The computation of the effective conductivity was made by the finite element method using the commercial software COMSOL. The binary images were converted to meshes by a partially self-written code. In the first step ordered lists containing the coordinates of the pixels belonging to a connected piece of boundary were generated. Each such list represents a polygonal approximation of the boundary of a connected piece of the metal phase. The second step is to fill the interior of these polygons with a triangular mesh. After setting the boundary values the Poisson equation was solved by the software. The standard direct solver for the linear system was used. All images and their backbones were used to solve two boundary value problems: one for the setup where the horizontal conductivity is measured and one for the vertical setup.

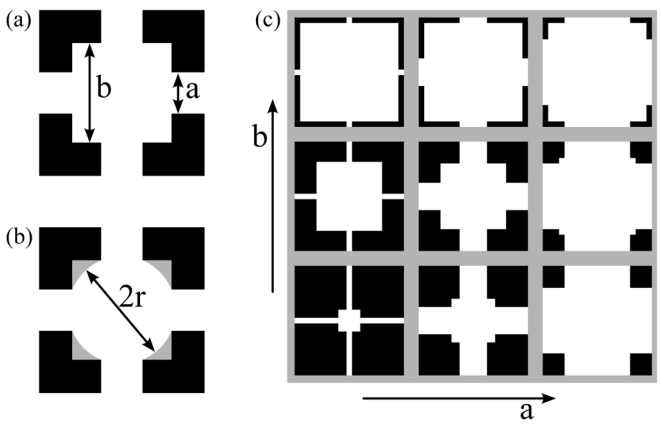

FIG. 4. (a) A simple two-parameter family of sets representing the microstructure of a metal-insulator composite consisting of a single percolating cluster. (b) Backbone according to the definition given in Eq. (10) with dead-ends shown in gray. (c) Illustration of the sets obtained for small, middle and large values of the two parameters a and b.

The square symmetric sets and their backbones were generated by union of rectangles and disks. A script sweeping the two parameters, as detailed above, generated the samples, set the boundary values and solved the Poisson equation automatically.

For every sample and its backbone the area fraction of the metal phase was computed from the mesh representation that was used to solve the boundary value problem.

B. Image filter extracting the backbone

The image filter we present is composed of different traditional image processing operations. In Sec. III it is shown that the image filter introduced only slightly decreases the effective conductivity. We therefore call the filter Backbone (BB). All image processing operations used were implemented from scratch in C++ to allow incorporation of modifications of these operations. The labeling of clusters of white pixels is done by the algorithm originally proposed by Hoshen and Koopelman.[27] A cluster is considered to percolate the image window, if it connects to all four edges. White pixels need to share an edge to be considered connected, while black pixels are considered connected if they share at least a corner. As a consequence of these requirements, in two dimensions the percolating cluster (PC) is unique, if it exists. The Euclidean distance transform (EDT) was implemented according to the algorithm of Saito and Toriwaki.[28] It assigns to each white pixel the Euclidean distance to the next black pixel. Finally the computation of the skeleton by influence zones (SKIZ) is based on the algorithm published by Soille and Vincent.[29] Here the clusters of black pixels are considered water basins and the EDT values of the white pixels as height of a mountain landscape. The watersheds of this landscape are the SKIZ of the white pixels, they are formed by those crests that separate different basins. The basins must be labeled using 8-connectivity, since the white pixels are subject to 4-connectivity. For our purpose it was necessary to add to the SKIZ all white pixels which lie along the boundary of the image. This makes sure that the SKIZ of a percolating cluster is again a percolating cluster, see bottom right in Fig. 5. We denote this operation by SKIZb, standing for skeleton by influence zone with boundary. To obtain the

FIG. 5. (Color online) The backbone (BB), shown in yellow, is the union of maximal disks centered on the percolating part of the SKeleton by Influence Zones with boundary (SKIZb), here shown in orange. For the green SKIZb-pixel the maximal disk associated with it is shown.

backbone we composed the above mentioned filters in the following way

$$\mathrm{BB}: M \subset W \mapsto M_{\mathrm{BB}} \subset M,$$
$$M_{\mathrm{BB}} = \bigcup_{p \in \mathrm{PC} \circ \mathrm{SKIZb}(M)} b_{\mathrm{EDT}(M)|_p}(p), \tag{10}$$

where $b_{\mathrm{EDT}(M)|_p}(p)$ is the maximal disk contained in M centered at the point p. The formula states that the BB is the subset of the white pixels which is covered by maximal disks sitting on the percolating cluster of the SKIZb. This is shown schematically in Fig. 5. The less metal pixels are present in the input image, the faster is the computation of image transformations. Thus extracting the percolating cluster of the metal phase before proceeding as given by Eq. (10) will speed up the computation of the backbone for many cases.

Typically the above filter results in loss of boundary pixels. This is a severe drawback, if the metal phase consists of structures that are only few pixels wide. To circumvent this problem, we dilate the set obtained from the above filter with a 3×3 structuring element, this amounts to adding a one pixel thick layer of white pixels at all boundaries between white and black pixels. Then we intersect this image with the input image to make sure that the result is a subset of the input set. For very fine structures however pixels sharing only a corner with the pixels of the backbone are added in this step, so another application of the filter extracting the percolating cluster is needed. In formulae this reads

$$\tilde{M}_{\mathrm{BB}} = \mathrm{PC}(\delta_{3\mathrm{x}3}(M_{\mathrm{BB}}) \cap M). \tag{11}$$

For all binary images we use $\tilde{M}_{\mathrm{BB}}$, but we drop the tilde from now on, since the difference between $\tilde{M}_{\mathrm{BB}}$ and M_{BB} is essentially a technical detail.

For the case of the two-parameter square symmetric sets described above, the backbone can be determined by hand from Eq. (10). The SKIZ is a simple cross made up of two lines. Taking the union of the maximal disks on this cross amounts to replacing the centered square of side length b with a disk of radius $r = (1/4)\sqrt{b^2 + a^2}$, as shown in Fig. 4(b).

III. RESULTS

The basic data for each sample and its backbone consists of the triple $\left(\sigma_e^{(ver)}, \sigma_e^{(hor)}, \phi\right)$ of effective conductivities in vertical setup, horizontal setup and the area fraction covered by metal. Therefrom the mean value of the effective conductivity

$$\sigma_e = \frac{1}{2}\left(\sigma_e^{(ver)} + \sigma_e^{(hor)}\right) \tag{12}$$

was computed. The relative difference for the conductivity in horizontal and in vertical setup ranges from 0 to 0.25 relative to the mean. Most samples show a relative difference smaller than 0.1. We will from now on only consider the mean conductivity of samples and their backbone, i.e., $\sigma_e(M)$ and $\sigma_e(M_{\mathrm{BB}})$ respectively, instead of the conductivities in horizontal and vertical setup.

In Fig. 6(a) the normalized mean conductivity of the samples represented by binary images is plotted versus the area fraction of metal. For each sample an asterisk shows the value $(\phi(M), \sigma_e(M)/\sigma)$ obtained from the unfiltered image. The dot shows the value $(\phi(M_{\mathrm{BB}}), \sigma_e(M_{\mathrm{BB}})/\sigma)$ obtained after passing the image through our filter. The dotted lines connect corresponding pairs. The dashed line shows the upper Hashin-Shtrikman bound, see Eq. (7). The dash-dotted line shows the curve for bond percolation on the square grid,[10] i.e., percolation threshold $\phi_c = 0.5$ and critical exponent $t = 1.3$ in Eq. (6). Figure 6(b) shows the plot for the pairs $(\phi, \sigma_e/\sigma)$ obtained from the two-parameter sets both filtered and unfiltered ones. As described in Sec. II the values of parameter a, the minimal width of the rods, are coarsely spaced. The values for parameter b, the side length of the central square, are narrowly spaced. Let's keep the value

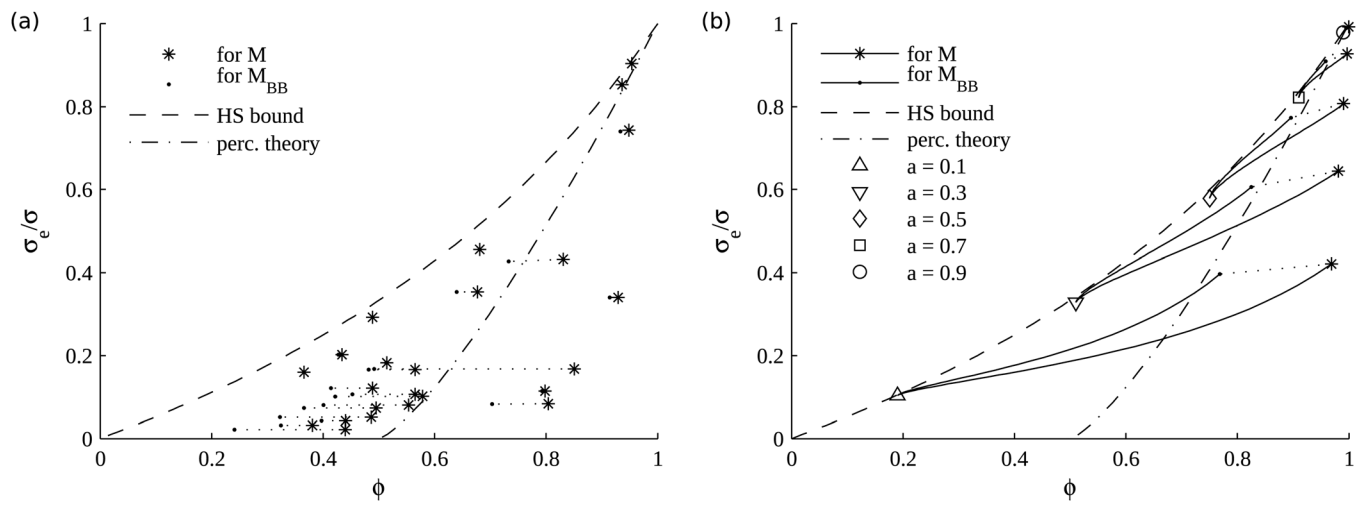

FIG. 6. (a) Normalized mean effective conductivity for samples of metal-insulator composites represented by binary images vs the area fraction covered by metal. The points $(\phi, \sigma_e/\sigma)$ plotted as asterisk were obtained from the unfiltered images and those plotted as dots from the backbones. The dotted lines connect corresponding pairs of unfiltered and filtered images. (b) Effective conductivity for the samples represented by the two-parameter sets vs area fraction. Each pair of curves joining at an open symbol is obtained from sets with parameter a fixed, see legend, and varying parameter b. See Fig. 4 for an illustration of the meaning of the two parameters.

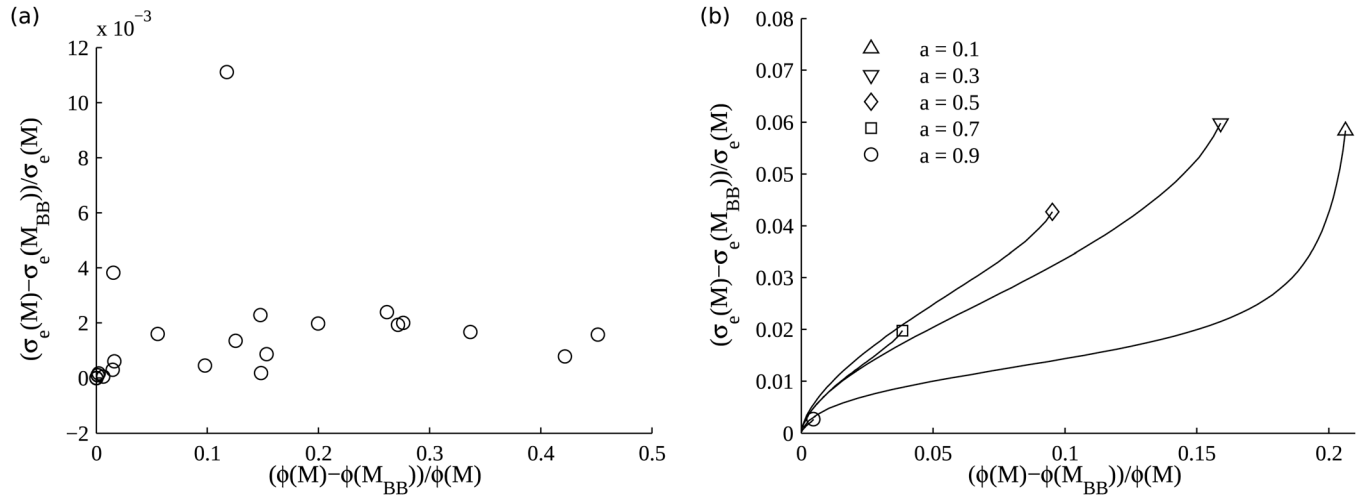

FIG. 7. Relative difference of the mean effective conductivity of the filtered and unfiltered samples. The data for the binary images is shown on the left side (a) and the data for the two-parameter sets on the right side (b). The x axis is the relative reduction of area fraction of metal when reducing the sample to its backbone. The curves in the plot in panel (b) correspond to varying parameter b and fixed value of parameter a, as indicated by the legend.

of a fixed for a moment. Varying parameter b the points $(\phi,\sigma_e/\sigma)$ range over a continuous curve once for the unfiltered set and once for its backbone. The open symbols code the value of a as indicated by the legend. At the minimal value of parameter b the set consists of a simple cross and thus is identical to its backbone. Furthermore it has minimal area fraction and conductivity. Thus the curves for the filtered and unfiltered sets meet at the side of small area fraction. For increasing values of b the area fraction and the conductivity increase and the unfiltered and filtered set become more and more different regarding area fraction. On the side of high area fraction each curve is marked with either an asterisk indicating that it corresponds to unfiltered sets or with a dot for the filtered sets. The curves for the unfiltered sets evidence that the majority of the area below the Hashin-Shtrikman bound is filled when the values of both parameter a and b are varied continuously in their admissible range. Surely, for $\phi = 1$ the range $0 \leq \sigma_e/\sigma < 1$ cannot be covered and if $\sigma_e = 0$ then necessarily $\phi = 0$ for the sets of the two parameter family.

The relative difference between the effective conductivity of the filtered and unfiltered sample is shown in Fig. 7 for every sample. The x-axis in this plot is the relative change of area fraction induced by the filter. Samples which are almost identical to their backbone are located at small relative change of area fraction. The relative difference in effective conductivity for the samples represented by binary images, shown in Fig. 7(a), is in the range of a couple of per mill. Only one sample yields a relative change in effective conductivity in the range of one percent. It is the third from left in the last row of Fig. 3. This observation is discussed in more detail in Sec. IV. Again for the samples represented by two-parameter sets each chosen value of a yields a continuous curve for varying b. Notice that in this case the relative difference in effective conductivity increases with increasing relative change of area fraction induced by the backbone.

In Fig. 8, the ratio between the effective conductivity of each sample and the Hashin-Shtrikman bound was computed once using the area fraction of the unfiltered sample and once using the area fraction of the backbone. The ratio of the

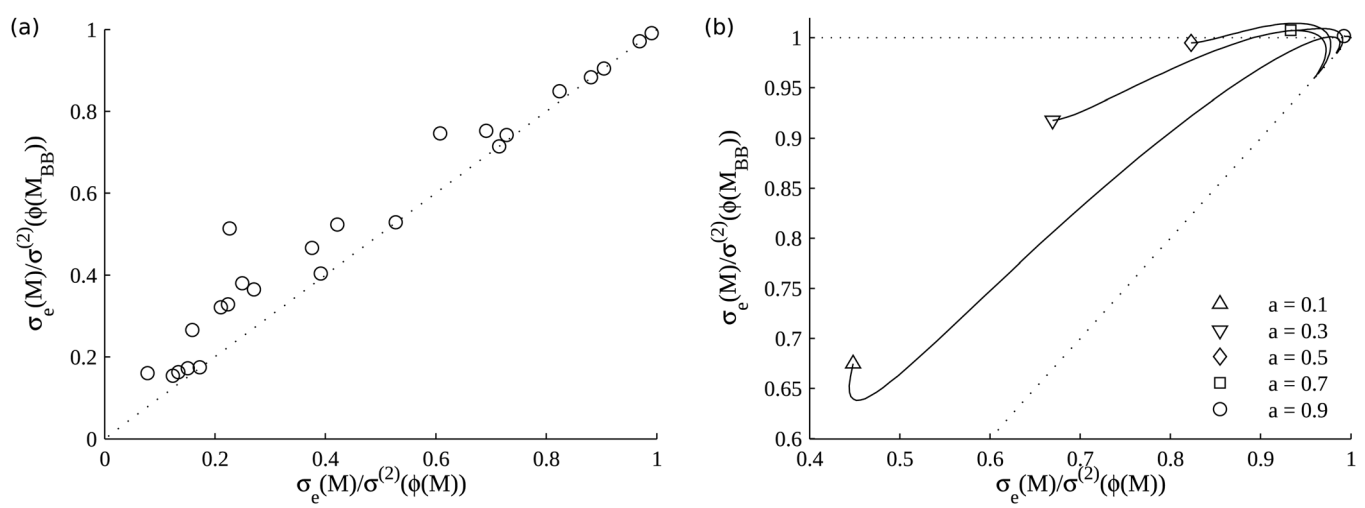

FIG. 8. The ratio of the effective conductivity and the Hashin-Shtrikman bound evaluated using the area fraction of the backbone is shown vs the ratio of the effective conductivity evaluated at the area fraction of the sample as is. (a) The data for the binary images. (b) The data for the two-parameter sets.

effective conductivity of a sample to the value of the Hashin-Shtrikman bound [Eq. (7)] computed from the area fraction of the backbone, i.e., $(\sigma_e(M))/(\sigma^{(2)}(\phi(M_{\mathrm{BB}})))$ is plotted versus the ratio of the effective conductivity to the value of the Hashin-Shtrikman bound evaluated at the area fraction of the unfiltered sample, i.e., $(\sigma_e(M))/(\sigma^{(2)}(\phi(M)))$. The meaning of these expressions will be discussed in Sec. IV. Fig. 8(a) shows the plot for the samples represented by binary images. All data points lie above the diagonal (dotted line) and are smaller than one. The corresponding plot for the samples represented by the two-parameter sets is shown in Fig. 8(b) where again all values are above the diagonal (dotted line), but here some values larger than one occur.

All samples represented by a binary image were used to generate two other images by filtering once and twice. For every sample their difference was then computed. It was found for all studied samples that the second application of the BB filter did not change the once filtered image.

IV. DISCUSSION

In this section speaking of the "backbone" we mean the image filter BB: $M \mapsto M_{\mathrm{BB}}$, as defined by Eq. (10), as well as the resulting set M_{BB}.

We will first discuss the change in the effective conductivity induced by the backbone. The backbone is always a subset of the sample itself, i.e., $M_{\mathrm{BB}} \subset M$. This implies that the effective conductivity of the backbone is a lower bound for the effective conductivity of a sample, i.e.

$$\sigma_e(M) \geq \sigma_e(M_{\mathrm{BB}}), \quad \forall M. \tag{13}$$

In other words the error in conductivity induced by reducing the sample to its backbone $\sigma_e(M) - \sigma_e(M_{\mathrm{BB}})$ is never negative. This implies that the errors obtained for the horizontal and vertical setup cannot cancel each other when taking the mean of the conductivity from these two setups, Eq. (12). For most of the samples represented by the binary images the relative error in mean conductivity is below 0.3% as can be seen in Fig. 7(a). The one data point close to 1.2% stems from the binary image with the "line stars" (third from right in the bottom line in Fig. 3). The sharp corners close to the star centers are chopped off by the backbone. The sum of the current density in these regions appears to be considerably large. Still the data shows that the conductivity of the samples and the respective backbones are very close. This is what the name backbone refers to: electrical conductivity is essentially sustained by the backbone. The plot in Fig. 7(a) shows the relative error versus the relative reduction of area induced by the backbone. There is no apparent correlation between the error and the area reduction, thus it is less important how much metal is removed rather than where it is removed from.

In the case of the samples represented by the two-parameter family of square symmetric sets (see Fig. 4) the relative error in conductivity reaches values up to 7%, see the plot in Fig. 7(b). This is significantly larger than for the case of the binary images (Fig. 3). The reason is that the corner parts of the central square are not retained by our backbone as illustrated in Fig. 4(c). However, the current density in these "dead-ends" seems to be quite large. The effect is more pronounced for sets with large change of area induced by the backbone, i.e. large value of parameter b (the side length of the central square). This shows that large step like changes in the width of a rod are primarily responsible for the change in effective conductivity after filtering with the BB. The sets of the two-parameter family range over microstructures which are worst case structures regarding the backbone. By cutting the sample as represented in Fig. 4(a) into four squares swapping positions over the diagonals and joining again to one big square an alternative representation looking like a Swiss cross is obtained. It can be shown by symmetry arguments that it is equivalent in terms of effective conductivity to the original representation. Interestingly this representation reveals the microstructural similarity to the sample with the star shaped inclusions (Fig. 3, bottom line, third from right) discussed earlier.

We now comment on the relation between conductivity and the area fraction of metal. The existence of a percolating cluster in the metal phase is a 0-1 criterion for the effective conductivity. If there is no percolating cluster the effective conductivity is necessarily zero, else it has an unknown positive value. If the area fraction is known, the effective conductivity is limited to the interval $\left[0, \sigma^{(2)}(\phi)\right]$, see Eq. (7). From Fig. 6 we see that the area fraction of metal in the backbone is not proportional to the effective conductivity: the data points $(\phi(M_{\mathrm{BB}}), \sigma_e(M_{\mathrm{BB}})/\sigma)$ scatter over a broad area. There can be well connected backbones with evenly distributed mass or such which have bottlenecks limiting the transport capacity. Nevertheless the backbone optimizes a given metal phase in the sense that the most wasted metal is removed. The remaining set is closer to the optimal one: the data points for the backbones lie closer to the Hashin-Shtrikman bound than those of the unfiltered samples.

Fig. 8 shows plots of the data where the x-axis is a measure for how efficiently the metal present in the sample contributes to the effective conductivity. If the value of $(\sigma_e(M))/(\sigma^{(2)}(\phi(M)))$ is one, the microstructure M is optimal in the following sense. For given metal content $\phi(M)$ there is no microstructure with an effective conductivity larger than σ_e (M). Knowing that only the backbone M_{BB} carries significant current we interpret $\sigma^{(2)}(\phi(M_{\mathrm{BB}}))$ as an estimator for the effective conductivity $\sigma_e(M)$ of the metal insulator M. Now the y-axis of the plots in Fig. 8 has the meaning of the accuracy of this estimator. Values below one indicate an overestimation of the effective conductivity, whereas values larger than one indicate underestimation of the effective conductivity. The dotted line shows the quality of the Hashin-Shtrikman bound when interpreted as an estimator for the effective conductivity. The data points in Fig. 8 in general lie above the diagonal, this means that $\sigma^{(2)}(\phi(M_{\mathrm{BB}}))$ is closer to the true value $\sigma_e(M)$ than the Hashin-Shtrikman bound is. Thus using the area fraction of the backbone leads to an improved estimator for the effective conductivity based on the Hashin-Shtrikman bound. However, many of the values of the quality are well below one. So this representation of the data clearly shows that the mass of the backbone can be distributed more or less

efficiently regarding transport. The less efficiently the metal is distributed regarding conductivity, the more off is the estimated value for the conductivity.

As pointed out in Section ID, the notion of a dead-end is trivial if the criterion of no current flowing through it is applied strictly. Because the transition from "local broadening" of a rod to a long sidewards protrusion is continuous there is no canonical way to define the backbone. The longer a dead-end is, the smaller will the current density at its tip be. This suggests using a threshold for the current density in order to define which parts can be chopped off. However, this would require that the current density field were known and thus is not useful in the present context. In order to be easily computable the dead-ends and the backbone have to be defined by geometrical means. Our definition of the backbone and thus of dead-ends is based on image analysis and so is purely geometric. The image analysis operations used dictate the precise position of the cut between backbone and dead-end. The data of the effective conductivity for filtered and unfiltered images indicates that our definition is meaningful.

We finally comment on the observation that repeated application of the BB to all images studied here, resulted in no further change after the first application. We conjecture that this holds for any image, i.e., we argue that the BB is an idempotent set operation. From its definition we see that the BB is anti-extensive, i.e., it maps a set to a subset of itself. Together these two properties would make the BB a morphological filter.[30]

V. CONCLUSIONS

The classic definition of the backbone of a percolating cluster was extended with regard to identification of the electrically conducting backbone of two-dimensional metal-insulator composites. This allows to extract the backbone from any structure containing a percolating cluster. From a numeric study of the effective conductivity we conclude that the backbone filter frees a given structure from those parts which are irrelevant for its steady state DC transport properties. This opens the way for further geometrical characterization with the aim to develop a geometrical estimator for transport properties. For example, it would be interesting to investigate whether the microstructural characteristic ζ, mentioned in Sec. I C, can be used to construct a reasonably accurate estimator for the effective conductivity. An immediate idea is to compute $\zeta(M_{\mathrm{BB}})$, i.e., its value after filtering by the backbone. Together with $\phi(M_{\mathrm{BB}})$, the area fraction of metal after filtering, they could be inserted in either the three- or four-point bound [Eqs. (8),(9)] to obtain an estimate of the effective conductivity. The advantages of a purely geometric approach in contrast to the simulation of electrostatics are speed of the algorithms and lower memory requirement. Due to equivalence or similarity of the governing equations the backbone will also be useful to treat elasticity, thermal conductivity, transport by diffusion and fluid or gas flow in porous media.[8]

From the mathematical point of view our finding shows that it is possible to approximate the solution of a boundary value problem defined on a spatially complex set by the solution on a subset, which is in general less complex. This could help to push the limits of the size of systems that can be simulated.

ACKNOWLEDGMENTS

For their interest in the topic, the hint to Eq. (5) and helpful discussions the author would like to thank Prof. Camillo De Lellis and Elisabetta Chiodaroli from the Institute for Mathematics at the University of Zurich. The contact to them was initiated by Prof. Jürg Fröhlich at ETH Zurich, whose stimulating input during several discussions is also acknowledged. JR thanks his colleagues Henning Galinski, Pierre Elser, and Lukas Schlagenhauf for providing micrographs of dewetted Pt thin films [Fig. 1(a) and fourth from left in second line in Fig. 3]. Furthermore the author would like to thank Dr. Andreas Rüegg and Prof. Ralph Spolenak for their encouragement and hints to improve the manuscript. Finally, financial support by Gloor Instruments is acknowledged.

[1]M. Wang and N. Pan, Mater. Sci. Eng. R. **63**, 1 (2008).
[2]H. Huang, M. Nakamura, P. Su, R. Fasching, Y. Saito, and F. B. Prinz, J. Electrochem. Soc. **154**, B20 (2007).
[3]X. Wang, H. Huang, T. Holme, X. Tian, and F. Prinz, J. Power Sources **175**, 75 (2008).
[4]K. Sab, Eur. J. Mech. A/Solids **11**, 585 (1992).
[5]G. Milton, *The Theory of Composites*, Cambridge monographs on applied and computational mathematics; 6 (Cambridge University Press, Cambridge, 2002).
[6]J. D. Jackson, *Classical Electrodynamics* (Wiley, New York, 1990).
[7]J. C. Maxwell, *Treatise on Electricity and Magnetism* (Clarendon, Oxford, 1873).
[8]S. Torquato, *Random Heterogeneous Materials: Micro Structure and Macroscopic Properties* (Springer, New York, 2002).
[9]D. S. McLachlan, M. Blaskiewicz, and R. E. Newnham, J. Am. Ceram. Soc. **73**, 2187 (1990).
[10]D. Stauffer and A. Aharony, *Introduction to Percolation Theory* (CRC Press, Boca Raton, 1994).
[11]Z. Hashin and S. Shtrikman, J. Appl. Phys. **33**, 3125 (1962).
[12]Z. Hashin, *Theory of Composite Materials* (Pergamon, New York, 1970).
[13]S. Prager, Chem. Eng. Sci. **18**, 227 (1963).
[14]M. Beran, Nuovo Cimento **38**, 771 (1965).
[15]S. Torquato, "Microscopic Approach to Transport in Two-Phase Random Media," Ph.D. thesis, State University of New York at Stony Brook (1980).
[16]G. Milton, J. Appl. Phys. **52**, 5294 (1981).
[17]J. G. Berryman, J. Comput. Phys. **75**, 86 (1988).
[18]B. J. Last and D. J. Thouless, Phys. Rev. Lett. **27**, 1719 (1971).
[19]A. S. Skal and B. I. Shklovskii, Sov. Phys. Semicond. **8**, 1029 (1975).
[20]P. G. D. Gennes, J. Phys. Lett. **37**, L1 (1976).
[21]S. Kirkpatrick, AIP Conf. Proc. **40**, 99 (1978).
[22]R. Tarjan, SIAM J. Comput. **1**, 146 (1972).
[23]J. E. Hopcroft and R. E. Tarjan, Commun. ACM **16**, 372 (1973).
[24]D. C. H. H. J. Herrmann and H. E. Stanley, J. Phys. A **17**, L261 (1984).
[25]W.-G. Yin and R. Tao, Physica B **279**, 84 (2000).
[26]P. S. Jørgensen, "Quantitative Data Analysis Methods for 3d Micro Structure Characterization Of Solid Oxide Fuel Cells," Ph.D. thesis, technical university of Denmark (2010).
[27]J. Hoshen and R. Kopelman, Phys. Rev. B **14**, 3438 (1976).
[28]T. Saito and J.-I. Toriwaki, Pattern Recogn. **27**, 1551 (1994).
[29]L. Vincent and P. Soille, IEEE Trans. Pattern Anal. Mach. Intell. **13**, 583 (1991).
[30]P. Soille, *Morphological Image Analysis: Principles and Applications*, 2nd ed. (Springer, New York, 2004).